Received: 26 October 2023 | Revised: 24 January 2024 | Accepted: 18 February 2024

DOI: 10.1002/mp.17013

RESEARCH ARTICLE

MEDICAL PHYSICS

# Characterization of a flexible a-Si:H detector for in vivo dosimetry in therapeutic x-ray beams

**Matthew James Large**[1] | **Aishah Bashiri**[1,2] | **Yashiv Dookie**[3] | **Joanne McNamara**[3] | **Luca Antognini**[4] | **Saba Aziz**[5,6] | **Lucio Calcagnile**[5,6] | **Anna Paola Caricato**[5,6] | **Roberto Catalano**[7] | **Deborah Chila**[8,9] | **Giuseppe Antonio Pablo Cirrone**[7] | **Tomasso Croci**[10] | **Giacomo Cuttone**[7] | **Sylvain Dunand**[4] | **Michele Fabi**[8,11] | **Luca Frontini**[12] | **Catia Grimani**[8,11] | **Maria Ionica**[10] | **Keida Kanxheri**[10,13] | **Valentino Liberali**[12] | **Martino Maurizio**[5,6] | **Giuseppe Maruccio**[5,6] | **Giovanni Mazza**[14] | **Mauro Menichelli**[10] | **Anna Grazia Monteduro**[5,6] | **Arianna Morozzi**[10] | **Francesco Moscatelli**[10,15] | **Stefania Pallotta**[8,9] | **Daniele Passeri**[10,16] | **Maddalena Pedio**[10,15] | **Giada Petringa**[7] | **Francesca Peverini**[10,13] | **Lorenzo Piccolo**[14] | **Pisana Placidi**[10,16] | **Gianluca Quarta**[5,6] | **Silvia Rizzato**[5,6] | **Federico Sabbatini**[11,8] | **Leonello Servoli**[10] | **Alberto Stabile**[12] | **Cinzia Talamonti**[8,9] | **Jonathan Emanuel Thomet**[4] | **Luca Tosti**[10] | **Mattia Villani**[8,11] | **Richard James Wheadon**[14] | **Nicolas Wyrsch**[4] | **Nicola Zema**[10,17] | **Marco Petasecca**[1]

[1]Centre for Medical Radiation Physics, University of Wollongong, Wollongong, New South Wales, Australia

[2]School of Physics, Najran University, Najran, Saudi Arabia

[3]Shoalhaven Cancer Care Centre, Nowra, New South Wales, Australia

[4]Ecole Polytechnique Fédérale de Lausanne (EPFL), Photovoltaics and Thin-Film Electronics Laboratory (PV-Lab), Neuchâtel, Switzerland

[5]INFN Sezione di Lecce, via per Arnesano, Lecce, Italy

[6]Department of Mathematics and Physics "Ennio de Giorgi", University of Salento, Via per Arnesano, Lecce, Italy

[7]INFN Laboratori Nazionali del Sud, Catania, Italy

[8]INFN Sezione di Firenze, Florence, Italy

[9]Department of Experimental and Biomedical Clinical Science "Mario Serio", University of Florence, Florence, Italy

[10]INFN Sezione di Perugia, Perugia, Italy

[11]DiSPeA, Università di Urbino Carlo Bo, Urbino, Italy

[12]INFN Sezione di Milano, Via Celoria 16, Milan, Italy

[13]Dip. di Fisica e Geologia dell'Università degli Studi di Perugia, Perugia, Italy

[14]INFN Sezione di Torino, Turin, Italy

[15]CNR-IOM, Perugia, Italy

[16]Dip. di Ingegneria dell'Università degli studi di Perugia, Perugia, Italy

[17]CNR Istituto struttura della Materia, Rome, Italy

**Correspondence**
Marco Petasecca, Centre for Medical Radiation Physics, University of Wollongong, Wollongong, NSW 2522, Australia.
Email: marcop@uow.edu.au

## Abstract

**Background:** The increasing use of complex and high dose-rate treatments in radiation therapy necessitates advanced detectors to provide accurate dosimetry. Rather than relying on pre-treatment quality assurance (QA) measurements alone, many countries are now mandating the use of in vivo dosimetry, whereby a dosimeter is placed on the surface of the patient during treatment. Ideally, in vivo detectors should be flexible to conform to a patient's irregular surfaces.

**Purpose:** This study aims to characterize a novel hydrogenated amorphous silicon (a-Si:H) radiation detector for the dosimetry of therapeutic x-ray beams. The detectors are flexible as they are fabricated directly on a flexible polyimide (Kapton) substrate.

**Methods:** The potential of this technology for application as a real-time flexible detector is investigated through a combined dosimetric and flexibility study. Measurements of fundamental dosimetric quantities were obtained including output factor (OF), dose rate dependence (DPP), energy dependence, percentage depth dose (PDD), and angular dependence. The response of the a-Si:H detectors investigated in this study are benchmarked directly against commercially available ionization chambers and solid-state diodes currently employed for QA practices.

**Results:** The a-Si:H detectors exhibit remarkable dose linearities in the direct detection of kV and MV therapeutic x-rays, with calibrated sensitivities ranging from (0.580 ± 0.002) pC/cGy to (19.36 ± 0.10) pC/cGy as a function of detector thickness, area, and applied bias. Regarding dosimetry, the a-Si:H detectors accurately obtained OF measurements that parallel commercially available detector solutions. The PDD response closely matched the expected profile as predicted via Geant4 simulations, a PTW Farmer ionization chamber and a PTW ROOS chamber. The most significant variation in the PDD performance was 5.67%, observed at a depth of 3 mm for detectors operated unbiased. With an external bias, the discrepancy in PDD response from reference data was confined to ± 2.92% for all depths (surface to 250 mm) in water-equivalent plastic. Very little angular dependence is displayed between irradiations at angles of 0° and 180°, with the most significant variation being a 7.71% decrease in collected charge at a 110° relative angle of incidence. Energy dependence and dose per pulse dependence are also reported, with results in agreement with the literature. Most notably, the flexibility of a-Si:H detectors was quantified for sample bending up to a radius of curvature of 7.98 mm, where the recorded photosensitivity degraded by (–4.9 ± 0.6)% of the initial device response when flat. It is essential to mention that this small bending radius is unlikely during in vivo patient dosimetry. In a more realistic scenario, with a bending radius of 15–20 mm, the variation in detector response remained within ± 4%. After substantial bending, the detector's photosensitivity when returned to a flat condition was (99.1 ± 0.5)% of the original response.

**Conclusions:** This work successfully characterizes a flexible detector based on thin-film a-Si:H deposited on a Kapton substrate for applications in therapeutic x-ray dosimetry. The detectors exhibit dosimetric performances that parallel commercially available dosimeters, while also demonstrating excellent flexibility results.

**KEYWORDS**
flexible dosimetry, hydrogenated amorphous silicon, radiation detection

## 1 | INTRODUCTION

Quality Assurance (QA) in advanced EBRT modalities has become increasingly challenging for standard detector technologies. Traditionally, QA in EBRT is performed before treatment using standardized dose measurements obtained by ionization chambers in water or water-equivalent phantoms.[1] While these provide adequate verifications for treatment planning, pre-treatment QA cannot account for differences in patient geometry between planning and treatment stages, nor can it monitor any deviations in the actual clinical dose during delivery. In this regard, real-time dosimetry is essential. As outlined by Prabhakar et al.,[2] real-time dosimetry for treatments with a linear accelerator (LINAC) can be provided at four distinct points: the collimator, the patient, the couch, and finally through electronic portal imaging devices (EPIDs). This ability to provide real-time verification of the dose delivered to the patient is known as in vivo dosimetry.

In vivo dosimetry is fast becoming a compulsory component of QA practices for external beam radiotherapy. Throughout many European countries, in vivo dosimetry is now mandatory as per the Medical Exposure Directive (MED) 97/43/Euratom.[3] In vivo dosimetry is most beneficial in treatment modalities where the treatment planning system may have more uncertainty, such as irradiations delivered at shallow depths and total body irradiations. Regardless, in vivo dosimetry provides a direct means of verifying the delivered dose, which can aid in minimizing the risk of improper dose delivery that causes severe injury or, in extreme cases, death.[4]

Detectors must meet several burdensome requirements to be able to perform real-time in vivo dosimetry, such as being accurately able to measure skin dose or dose in the build-up region, being flexible as to conform to the patient's treatment area, providing an angular independent response, and be transparent enough to provide minimal perturbations to the treatment beam.

Several current technologies provide solutions to the challenges mentioned above. Radiochromic films are flexible and provide excellent tissue equivalence, spatial resolution, and the ability to perform dosimetry over a large area.[5] However, film-based dosimetry is a passive technology that cannot provide the desired real-time feedback. For real-time large-area dosimetry, several solutions are available based solely on EPID or a combination of EPID and dedicated detectors, such as the solution proposed by Brace et al.[6] These large-area pixelated detectors typically employ a 2D array of silicon detectors placed on the flat panel imager available on most clinical LINACs to monitor exit dose during patient treatments. Olaciregui-Ruiz et al.[7] provide an extensive review of the requirements of EPID dosimetry. For real-time dosimetry that is accurate and free of complex tissue-equivalent correction factors, limitations arise due to the high-Z semiconductor materials typically employed in fabricating EPIDs, MOSFETs, and other solid-state dosimeters. Furthermore, many of these commercially available solutions lack the flexibility required to conform to the patient surface.[7] Fiber optic and organic semiconductor detectors are examples of unique solutions that provide both flexibility and improved tissue-equivalence. However, both technologies rely on the indirect detection of x-rays facilitated by scintillators. Often, these scintillators cause the generation of parasitic signals due to photoluminescence or Cerenkov radiation, which traditionally resulted in a reduction in the spatial resolution and dosimetric accuracy of these technologies.[8–10] Modern radioluminescent dosimeters point or multi-point for in vivo dosimetry can mitigate or apply correction factors to account for these limitations, resulting in accurate full-field in vivo dosimetry from real-time scintillator-based detectors.[11,12] An angular independent detector response is highly desirable in the case of rotating or robotic EBRT delivery modalities (such as volumetric modulated arc therapy (VMAT), Tomotherapy, and Cyberknife) where irradiations occur from multiple angles. Devices such as the "Edgeless" silicon detector have been proven to provide a viable solution but still lack flexibility and have a radiation tolerance limited by their crystalline silicon bulk.[13] In summary, new detector technologies providing accurate real-time patient dosimetry would be beneficial to address all the challenges offered by advanced treatment modalities.

Hydrogenated amorphous silicon (a-Si:H) is an attractive solution for in vivo skin dosimetry for therapeutic x-ray fields. This material, fabricated via Plasma-Enhanced Chemical Vapour Deposition (PECVD) can be deposited over large areas (such as 6 and 12-inch diameter wafers) and onto various substrates, including mechanically flexible materials such as Polyimide (Kapton). Traditionally, the use of a-Si:H stems from the solar cell industry, where diode structures possess layers with thicknesses on the order of hundreds of nanometers. By combining commercially available a-Si:H solar cells with scintillator screens, Jeong et al.[14] describes a complete a-Si:H dosimetry system for therapeutic x-rays. However, this system cannot be considered flexible, as the scintillator screen is a 1 mm thick slab containing gadolinium oxysulfide (GOS). Furthermore, the dosimetric performance of the system is heavily influenced by perturbations in the beam caused by the scintillator screen, evident particularly in the percentage depth dose (PDD) and output factors (OF) measured by the system.[14]

The addition of hydrogen to a-Si (from 4% to 10% atomic) passivates the effect of most of the dangling bonds (DBs), reducing the defect density within the amorphous silicon structure and reducing

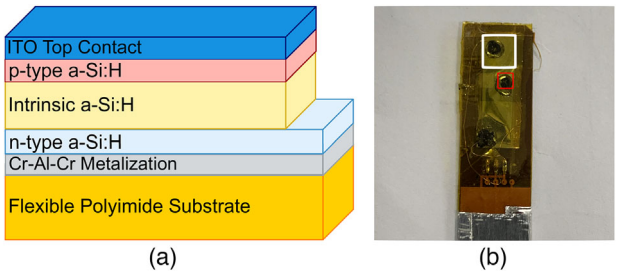


**FIGURE 1** (a) Schematic of the detector architecture. Image layers are not to scale. (b) Image of fabricated detectors showing pixel area variations of $2 \times 2$ mm$^2$ (red outline) and $5 \times 5$ mm$^2$ (white outline).

recombination cross sections. Reducing the concentration of DBs improves the material mobility and provides a nearly intrinsic substrate that enables the fabrication of n-i-p diodes.[15] In this work, we explore using a thin film a-Si:H diode structure that removes the need for coupling with a scintillator to measure x-ray dose. Although thicker than their solar cell predecessors, these detectors still possess a thin intrinsic layer (a few microns) and thin (tens to hundreds of nanometers) doped layers. Notably, the film thickness is still sufficient to detect kV and MV x-rays with an appropriate sensitivity directly. This removes the need to couple the detector to a scintillating material, resulting in fully flexible devices. The authors' previous work, under the INFN HASPIDE project, has successfully demonstrated the use of a-Si:H in high-flux beam monitoring applications such as those required for dosimetry for Microbeam Radiation Therapy (MRT).[16] Here, we characterize the use of an improved version of the same a-Si:H technology for dosimetry in kV and MV fields. These improvements include fabricating the detectors on flexible, water-equivalent substrates and adopting carbon-based electrical contacts rather than silver-based contacts that have been shown to cause dose-enhancements.[16]

## 2 | METHODOLOGY

### 2.1 | Detector design and fabrication

The investigated detectors are a-Si:H planar pad diode structures fabricated on a mechanically flexible polyimide (Kapton) substrate. Detectors were manufactured by the PV-Lab at École Polytechnique Fédérale de Lausanne (EPFL), Neuchâtel, Switzerland. A Cr-Al-Cr layer is deposited directly onto a 125-μm polyimide substrate using a Leybold UNIVEX sputter coating system. The a-Si:H n-i-p diode layers are then deposited through PECVD at a temperature of 200°C. For the top electrical contact, a 28 nm Indium-Tin-Oxide (ITO) layer is deposited via sputtering, interfacing directly with the *p*-doped layer of the a-Si:H n-i-p stack. Finally, a dry etch is performed to remove the *p*-type layer of a-Si:H between the ITO pads and create isolation between neighboring pixels. The resulting structures are single n-i-p diode pixels (Figure 1a), each with an intrinsic layer thickness of either 2.5 or 5 μm and sensitive pixel areas of either $2 \times 2$ mm$^2$ or $5 \times 5$ mm$^2$. The pitch between neighboring $2 \times 2$ mm$^2$ pixels is 0.5 mm edge-to-edge, with the larger $5 \times 5$ mm2 pixel situated 1 mm above the smaller pixels (Figure 1b). The detector dimensions used in this study were selected from a larger production batch of detectors ranging in sizes from $1 \times 1$ up to $10 \times 10$ mm$^2$. The pixels sizes of $2 \times 2$ and $5 \times 5$ mm$^2$ were selected as their responses were stable, low noise, and reproducible. The intensity of the kV and MV x-ray fields restricted the use of the smallest $1 \times 1$ mm$^2$ pixels, as the active area was too small to produce a reliable response with a sufficient signal-to-noise ratio. Conversely, the largest $10 \times 10$ mm$^2$ pixel area detectors would cause a large volume-averaging effect for angular dependence and OF measurements.

**TABLE 1** Nomenclature of a-Si:H on Kapton detector types.

| a-Si:H Layer thickness | Pixel area (mm$^2$) | Detector architecture ID |
|---|---|---|
| 2.5 μm | $2 \times 2$ | aSiH-KAP2S |
| | $5 \times 5$ | aSiH-KAP2L |
| 5 μm | $2 \times 2$ | aSiH-KAP5S |
| | $5 \times 5$ | aSiH-KAP5L |

Abbreviation: a-Si:H, hydrogenated amorphous silicon.

For easier referencing, the four detector variants can be referred to via a unique identifier of the form *aSiH-KAP**XY***, where the last two characters of the ID refer directly to the active layer thickness and sensitive area, respectively. Table 1 provides the details of this nomenclature.

Figure 1b displays the sensor assembled on a flexible Kapton tail (35 cm long). Electrical contact is facilitated by a carbon-based conductive paint (MG Chemicals 838AR) encapsulated with epoxy glue for mechanical rigidity. The carbon-based coating is employed as previous studies using silver-based conductive paint demonstrated significant dose-enhancement facilitated by the silver contacts, particularly in high dose rates and soft x-ray beams.[16] This study's resulting flexible a-Si:H dosimeters are the second generation produced within the HASPIDE project. Previous generations of the HASPIDE flexible a-Si:H detector have been successfully characterized for x-ray dosimetry applications by Talamonti et al.[17] For a more detailed description of the device design and fabrication process, see Menichelli et al.[18]

The tail facilitates real-time readout of the detector pixels using a multichannel electrometer developed in-house by the Centre of Medical Radiation Physics (CMRP) at the University of Wollongong, Australia.[19]

## 2.2 | Sensitivity to MV x-rays

To assess the sensitivity of the a-Si:H detectors to MV x-rays, the detectors were irradiated using 6 MV x-rays produced by a Varian Clinac 21iX LINAC at the Shoalhaven Cancer Care Centre (SCCC). This LINAC operates with nominal pulse-rate and pulse width values of 360 Hz and 3.6 μs, respectively. Under reference dosimetry conditions, these settings produce an instantaneous dose of $2.78 \times 10^{-4}$ Gy/Pulse. For dosimetry and QA measurements, reference conditions are defined for a detector placed at the depth of maximum dose in a water-equivalent plastic (solid water) phantom ($d_{max} = 1.5$ cm) where the source-to-surface distance (SSD) of the phantom is at isocenter (100 cm SSD) for a $10 \times 10$ cm$^2$ field size. In addition to 1.5 cm of build-up, 10 cm of backscatter material is used. Under reference conditions and with the LINAC operated at a rate of 600 monitor units (MU) per minute, 1 MU is equivalent to a delivered dose of 1 cGy to the detector. All measurements conducted in this work are calculated as the average response (with background subtraction) from three repeated irradiations or exposures. The associated errors represent one standard deviation (SD) of these repetitions.

### 2.2.1 | Dose linearity and detector sensitivity

The dose linearity response was investigated for devices irradiated at reference dosimetry conditions for delivered doses from 20 up to 300 cGy. Results were recorded as the integral charge collected above the baseline for all detectors under passive (0 V) and biased (3 V) operation modalities. Detector aSiH-KAP5L was only operated at 0 V for the high current generated by the radiation for any applied bias, which was not compatible with the dynamic range of the data acquisition system. The sensitivity was calculated from the gradient of the resulting linear plots.

### 2.2.2 | Response versus bias

To further quantify the effect on the responsiveness of the detectors as a function of applied bias, measurements were conducted at applied biases from 0 to 6 V for detectors aSiH-KAP2S and aSiH-KAP5S. For each measurement, 100 MU (1 Gy) was delivered to detectors at reference conditions, and the resulting sensitivity (measured in pC/cGy) was plotted as a function of bias. According to Menichelli et al.,[20] the increase in device sensitivity for a-Si:H n-i-p diodes follows an inverted exponential trend with bias, which the following mathematical expression can describe:

$$I = p_0 * \left(1 - p_1 e^{-p_2 V}\right) \quad (1)$$

where $I$ is the detector current, $V$ is the applied bias voltage, and $p_0$, $p_1$, and $p_2$ are the calculated fit parameters. Using Equation (1) to fit the experimental data, the saturation voltage required for the total depletion of each device can be inferred $3/p_2$, where $p_2$ is the fit parameter from Equation (1)[20].

## 2.3 | Evaluating detector flexibility

For in vivo dosimetry, detectors may be required to operate whilst bent or deformed when conforming to the various surfaces of the human body such as the hand, arm, chest, or face. As a result, it is essential to quantify any variations in performance when detectors are bent. In this regard, an apparatus was developed to bend the a-Si:H detectors and record their response when illuminated with a monochromatic low-power laser producing visible light at 615 nm. The bending apparatus consists of two brass arms within which the sample can be held (Figure. 2a). Reducing the distance between the arms will result in a controlled bending of the detector. This is known as the "push-to-bend" or "push-to-flex" method,[21,22] commonly employed in flexible electronics testing.[23] A disadvantage of the push-to-bend method for device flexibility testing is the inability to directly measure and select the radius of curvature of the detector during measurements.[24] To calculate this, a high-definition camera is placed level with the detector whilst flat. A calibration image is taken with the detector flat and distance scale placed in a frame, allowing for image post-processing to convert from several pixels into millimeters (Figure 2b). After bending the detector, an ImageJ[25] macro was used to perform a circular fit to the curved detector and calculate the radius of curvature.

For bending radii between 152.38 and 7.98 mm, the detector response was normalized against the response when flat. Repeated illuminations were performed for each bending, with the response above background averaged and the associated error calculated as one standard deviation. Once a maximum bending radius of 7.98 mm was achieved, measurements were repeated at discrete intervals as the detector was returned to flat.

## 2.4 | Dosimetry for therapeutic x-ray beams

### 2.4.1 | Percentage depth dose (PDD)

PDD was investigated for all detector thickness and pixel area variations under biased and unbiased conditions. Measurements were taken for detectors irradiated with 100 MU (1 Gy) at depths from 0 up to 250 mm in

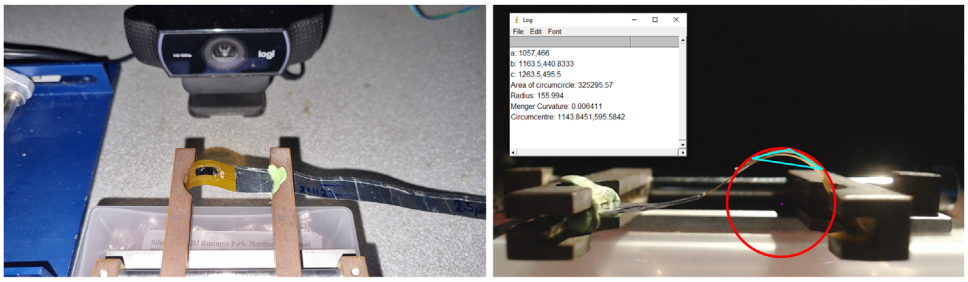


(a) (b)

**FIGURE 2** (a) Experimental set-up to measure bending radius and photosensitivity response of the detector, directly showing the bending of the detector on the Kapton read-out tail. (b) Image taken from the webcam with overlays showing the selected points on the bent detector (blue) and the fitting circle (red) calculated in ImageJ[25] to determine the radius of curvature.

solid water, controlled by introducing several slabs of solid water with a constant 10 cm of backscatter. An effective depth of approximately 150 μm was estimated for measurements at the surface based on the epoxy and polyimide tape thicknesses used to encapsulate the detectors. Measurements were recorded under reference dosimetry conditions (6 MV, 10 × 10 $cm^2$ field, 100 cm SSD) and normalized to the response at $d_{max}$ (15 mm).

The response of the a-Si:H detectors was compared directly to relative dosimetry measurements acquired with the PTW 30013 Farmer ionization chamber (Farmer IC) with 0.6 $cm^3$ sensitive volume. However, Farmer-type ionization chambers cannot accurately measure PDD at shallow depths. Therefore, the dose-profile of the build-up region (from surface to $d_{max}$) was obtained from Geant4 simulation data previously published by Vicoroski et al.[26] These simulations by Vicoroski et al. were performed in version 10.0.01 of Geant4 and modelled with the standard electromagnetic physics package activated. The simulation geometry was designed to precisely replicate the experimental conditions for detectors in a 30 × 30 × 30 cm3 water phantom and irradiated within a 10 × 10 $cm^2$ x-ray field at 100 cm SSD. For this, Vicoroski et al. employed a phase space file to generate the radiation field incident on the water phantom. This phase space file was created from a previously validated simulation[27] from a detailed model of the LINAC head a Varian 2100 series LINAC; identical to the LINAC used for experimental measurements at the Shoalhaven Cancer Care Centre in Wollongong (Australia). Vicoroski et al. scored the dose throughout the water phantom using 0.02 × 1 × 1 $mm^3$ voxels, and a step length and particle range cut length of 0.1 mm to reconstruct the PDD profile. Additional information regarding the simulation details from references 26 and 27 are provided in the supplementary information (Figure S2 and Table S1). For a more detailed description of the Geant4 simulation and data, see the publication of Vicoroski et al.[26]

For dosimetry measurements assessing absorbed dose to water, the International Atomic Energy Agency (IAEA) recommends using a plane-parallel IC for electron and photon EBRT.[28,29] Hence, PDD measurements were also obtained using the PTW Roos plane-parallel chamber for reference dosimetry. The Roos chamber PDD response was obtained in solid water for depths 3 to 250 mm to act as an accurate reference PDD response to benchmark the Farmer IC, Geant4 simulation data, and the a-Si:H detector responses.

### 2.4.2 | Dose per pulse (DPP)

The DPP dependency of a-Si:H detectors was investigated using aSiH-KAP5S (5 μm, 2 × 2 $mm^2$) operated at 3.5 V. As the LINAC is a pulsed radiation source, changing the output dose rate of the LINAC directly simply changes the number of pulses per second delivered. This change only alters the average dose rate and does not change the instantaneous dose rate delivered by each pulse. To modulate the dose-rate, the SSD of the detector can be changed. This method also avoids variations in the spectrum of incident photons.[30] At each SSD, the detector response is proportional to the total dose accumulated over several LINAC pulses. Therefore, the average DPP at each SSD was calculated by dividing the recorded dose by the number of LINAC pulses delivered. Measurements of the response of the aSiH-KAP5S detector and the Farmer IC were recorded for incident dose rates between 4.33 × $10^{-4}$ Gy/pulse and 2.53 × $10^{-5}$ Gy/pulse, corresponding to SSDs from 80 to 336.1 cm, respectively. The detector and IC responses were normalized to reference conditions (100 cm SSD). The results in Figure 3 show the ratio of the a-Si:H detectors SSD normalized response divided by the normalized IC response as a function of depth. Assuming that the ICs DPP dependence is within ± 1 %, as Wong et al. reported, any variations in the ratio

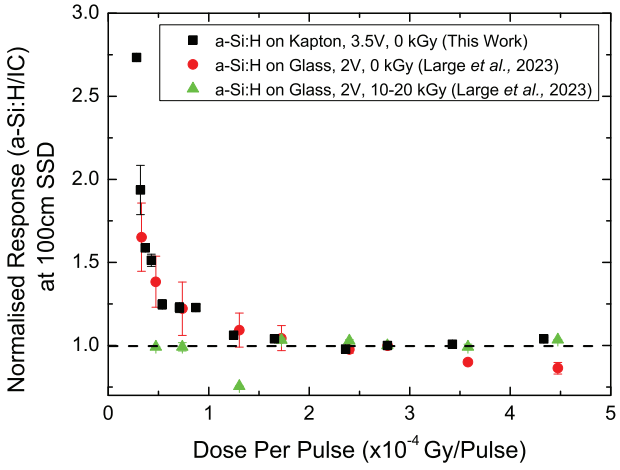


**FIGURE 3** Variation of photosensitivity of the a-Si:H detector under varying degrees of bending. A smaller radius of curvature indicates a greater degree of bending or strain applied to the detector. Data is given for the detector as bending increases (black squares), and the device is returned to flat (orange triangles).

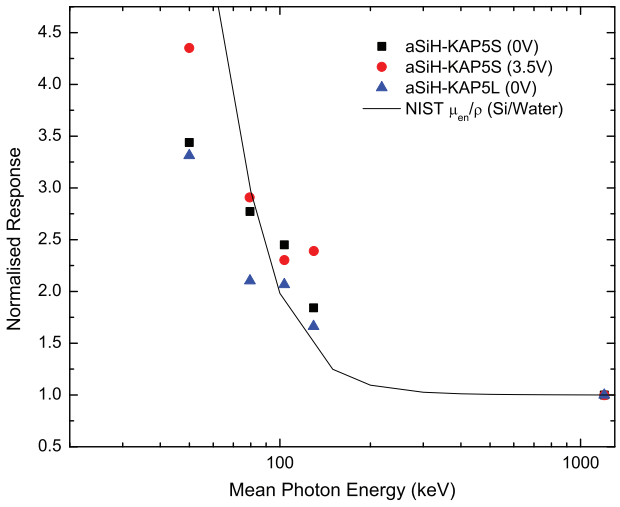


**FIGURE 4** PDD response of a-Si:H detectors with varying thicknesses, sensitive areas and applied biases. PDD dependencies are compared directly to CC13 data downstream of $d_{max}$ and to Geant4 simulation data from Vicoroski et al.[26] upstream of $d_{max}$. The PDD response of the PTW Roos detector is also provided for comparison. (a) Full PDD results and (b) zoom-in on the PDD response of detectors in the build-up region. All results are normalized to the response at $d_{max}$. PDD, percentage depth dose.

of detector response to IC response will indicate DPP dependencies in the a-Si:H detector.[31]

### 2.4.3 | Output factor

The OF is calculated as the dose per MU received at a selected field size normalized against the dose per MU received under reference conditions.[32,33] In this study, reference conditions were a field size of 10 × 10 $cm^2$ measured at a depth of 10 cm and with an SSD of 90 cm (isocenter). Field sizes ranging from 1 × 1 $cm^2$ up to 20 × 20 $cm^2$ were selected by controlling the aperture of the LINAC jaws.

Data obtained by commercially available ionization chambers from IBA Dosimetry was used to benchmark the a-Si:H performance. The CC13 was used for QA measurements for fields from 3 × 3 cm2 up to 20 × 20 $cm^2$, while the CC04 was used for 2 × 2 cm2 fields to avoid the volume average effects experienced by the CC13 at smaller fields. For comparisons to traditional film-based dosimetry as well as emerging solid-state silicon-based detectors, data from Petasecca et al.[13] collected on a Varian 2100iX at Illawarra Cancer Care Centre (ICCC) is used. This data is directly comparable as LINACs at SCCC are cross calibrated against the ICCC's LINACs. The work of Petasecca et al.[13] provides the OF response of EBT3 Gafchromic film and of a 0.5 × 0.5 $mm^2$ p-Si Edgeless detector for field sizes from 1 × 1 $cm^2$ up to 10 × 10 $cm^2$.

The ability of the a-Si:H detectors to accurately perform OF measurements for the selected field sizes will help identify any presence of volume averaging effects in these detectors. For a further assessment on how the pixel area affects the capability of these detectors to conduct field profiling measurements, Off-Axis Ratio (OAR) measurements are provided in the supplementary information (Figure S1).

### 2.4.4 | Angular dependence

A cylindrical rotatable phantom was used to investigate the angular dependence of the detectors. This phantom with a detector-specific insert ensures the detector is accurately placed at the LINAC isocenter and remains at a depth of 150 mm and an SSD of 85 cm, regardless of irradiation angle. The irradiation angle was selected from 0 to 180° in 10° increments by rotating the LINAC head while the detector remained stationary. Detector measurements are normalized to the response at 0° where the beam is perpendicularly incident on the surface of the detector. Conversely, an angle of 180° describes irradiation of the detector backside, with the LINAC field incident on the polyimide (Kapton) substrate. The work of Petasecca et al.[13] successfully validated using this cylindrical rotatable phantom for angular dependence measurements in MV fields. More details on conceptualizing the phantom and its intended use are also documented.[13]

### 2.4.5 | Energy dependence

Energy dependence measurements were performed using a Gulmay D3300 kilovoltage x-ray machine at

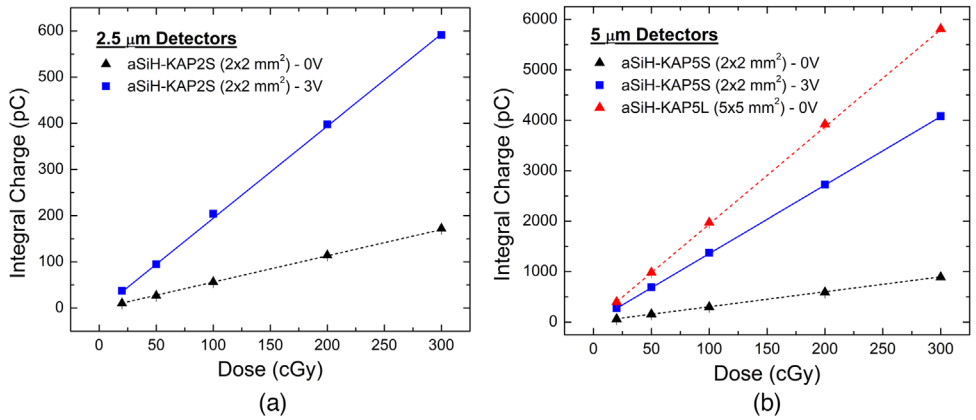


**FIGURE 5** DPP for aSiH-KAP5S (5 μm, 2 × 2 $mm^2$) under 3.5 V reverse bias (squares). Results are normalized to reference dosimetry conditions (100 cm SSD) and divided by the normalized IC response at each depth (a-Si:H/IC). Comparisons are made against previous generation a-Si:H detectors on glass, taken from Large et al.[16] The effect of pre-irradiation on detector responses is also investigated, with 0 kGy indicating no prior irradiations and 10–20 kGy signifying a pre-irradiated device. Error bars represent one SD. a-Si:H, hydrogenated amorphous silicon; DPP, dose per pulse; SSD, source-to-surface distance.

the ICCC. The accelerating voltage of the x-ray tube was set for potentials ranging from 100 up to 250 kVp, resulting in mean photon energies between 49.97 and 129.4 keV. At each of the selected mean photon energies, 100 MU was delivered, with the focus skin distances (FSDs) being either 30 or 50 cm, depending on the mean photon energy selected for irradiations. As the dose-rate of the kilovoltage machine varies with the selected kVp, independent dose verification measurements were first performed with the PTW pinpoint IC to calibrate the irradiation times and ensure deliveries of 100 MU. Furthermore, dose-rate correction factors were applied to the response of the a-Si:H detectors based on the DPP results presented in Figure 3.

Energy dependence was investigated for the aSiH-KAP5S detector for both passive (0 V) and biased (3.5 V) operations. Figure 4 displays the energy dependence of the detector (with dose-rate correction) normalized against the response when irradiated with 100 MU from the 6 MV Varian clinac, where the clinac delivers a mean photon energy of 1.2 MeV.

# 3 | RESULTS

## 3.1 | Sensitivity to MV x-rays

### 3.1.1 | Dose linearity

The response of the single pixel a-Si:H diodes was extremely linear within the 20 to 300 cGy range tested, with associated linear coefficients of determination ($R^2$) ranging from 0.9997 to 1. The dose linearity results are presented in Figure 5.

The calculated dose calibration factors of the detectors to 6 MV photons range from (0.580 ± 0.002) pC/cGy to (19.36 ± 0.10) pC/cGy (Table 2), as inferred from the linear responses in Figure 5.

### 3.1.2 | Response versus bias

The application of bias was observed to impact the dose calibration factors presented in Table 2 directly. To extend these observations, the relationship between the signal-to-dose calibration factor for 2 × 2 $mm^2$ detector pixels (detectors aSiH-KAP2S and aSiH-KAP5S) was measured for applied biases of up to 5 and 6 V for the 2.5 and 5 μm thick detectors, respectively.

The device sensitivities exponentially approach some saturation value with increasing bias, estimated as $3/p_2$ where $p_2$ is the fit parameter within the exponential as described by Equation (1) in Section 2.2.2. Applying this fit equation to each of the data series in Figure 6, the saturation voltages were calculated as (10.12 ± 0.73) V and (13.42 ± 2.89) V for detectors aSiH-KAP2S and aSiH-KAP5S, respectively.

## 3.2 | Evaluating detector flexibility

The normalized photosensitivity of detector aSiH-KAP5S as a function of the radius of curvature under which the detector is bent is detailed in Figure 7.

The detector response deviates less than ± 5 % for all bending radii tested compared to the detectors' photosensitivity when flat. At the most extreme bending case of a 7.98 mm bending radius of curvature, the detector photosensitivity was (−4.9 ± 0.6)% of the flat detector response. Realistically, for in vivo

**TABLE 2** Dose calibration factors as calculated from the linear trends of Figure 5.

| Detector ID | Thickness (μm) | Pixel area ($mm^2$) | Sensitivity at 0 V (pC/cGy) | Sensitivity at 3 V (pC/cGy) |
|---|---|---|---|---|
| aSiH-KAP2S | 2.5 | 2 × 2 | 0.580 ± 0.002 | 1.981 ± 0.021 |
| aSiH-KAP5S | 5 | 2 × 2 | 2.943 ± 0.015 | 13.56 ± 0.02 |
| aSiH-KAP5L | 5 | 5 × 5 | 19.36 ± 0.10 | – |

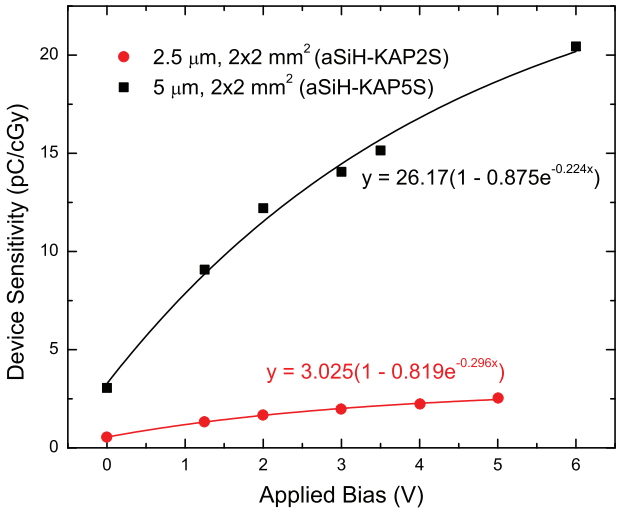


**FIGURE 6** OF for detector aSiH-KAP5S. All results are taken at 10 cm depth, 90 cm SSD, and normalized to the response under a 10 × 10 $cm^2$ field. The response of the CC04 and CC13 Ics (dotted line) are used as a benchmark for the detector performance. Error bars represent one SD. [a] The response of EBT3 film and an Edgeless *p*-Si detector are taken from Petasecca et al.[16]. OF, output factor.

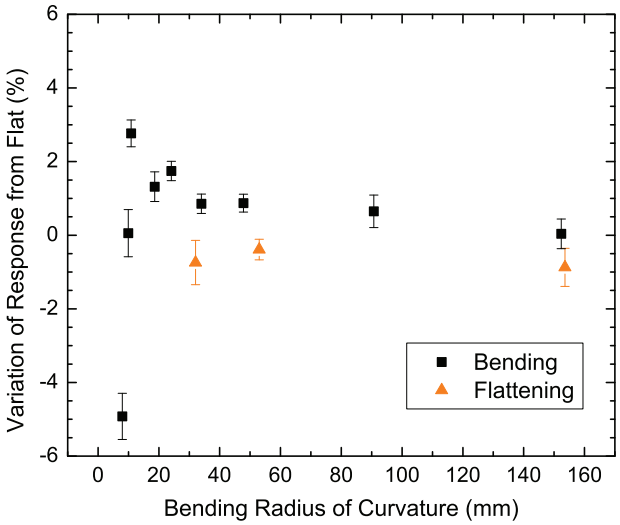


**FIGURE 7** Dose linearity results for (a) 2.5 μm and (b) 5 μm detector variants. Each figure shows results for biased (solid lines) and unbiased (dotted lines) operations. Error bars represent one SD from three repetitions at each point and are contained within the marker size.

applications, such small bending radii would never occur. With this practical limitation, the photosensitivity response varies by less than ± 3% between the response when flat and bending radii down to 10 mm. When returning to flat after bending, the photosensitivity of the detector returns to (99.1 ± 0.5) of its original flat response (i.e. a response variation of −0.9 ± 0.5% after bending).

## 3.3 | Dosimetry characterization for therapeutic x-ray beams

### 3.3.1 | Percentage depth dose (PDD)

The PDD response for three detector variants is shown in Figure 8. Results are benchmarked against the response of the reference Farmer IC for depths of 15 mm and greater, and against the Geant4 simulations calculated according to the method proposed by Vicoroski et al.[26] for the build-up region (surface to 15 mm). The response of the commercially available PTW Roos detector is provided for comparison. The subplot of Figure 8 provides the percentage difference between the performance of the detectors and the reference data at each depth.

An excellent agreement in the PDD response of a-Si:H detectors and the reference data is displayed in Figure 8. Upstream of $d_{max}$ (0–15 mm depths), the response from all investigated detectors vary by no more than ± 6 % from the Geant4 data of Vicoroski et al.[26] The most significant discrepancy is recorded as a 5.67% over-response at a 3 mm depth for aSiH-KAP5S at 0 V. Biased operation of the a-Si:H detectors appears to improve this response, with upstream deviations restricted to within ± 3% for detectors under 3 V reverse bias. Similarly, the biased detectors provide a response that more closely matches that of the CC13 downstream of $d_{max}$. The downstream response of biased detectors appears to stabilize about a 0% difference (Figure 8 subplot) for depths greater than 15 mm. In contrast, the unbiased detectors begin towards an under-response at around 100 mm. The most significant variation occurs again for an unbiased detector, with aSiH-KAP5L responding 4.41% below the CC13's response at a 200 mm depth. The response of the PTW Roos plane-parallel chamber is also provided in Figure 8, as the IAEA recommends using a

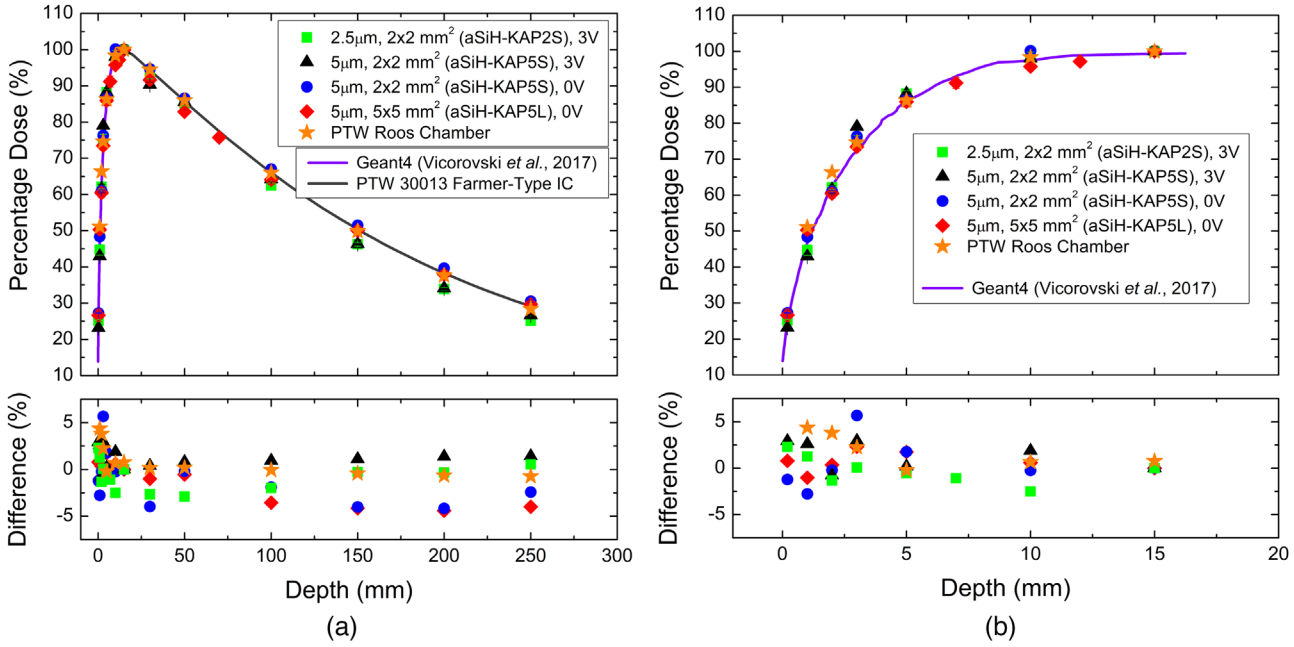


**FIGURE 8** Angular dependence of the 2.5 μm thick, 2 × 2 $mm^2$ a-Si:H detector (aSiH-KAP2S), with the direction of the x-ray field varying from normally incident (0°) on the face of the pixel to irradiating the pixel from the back of the device (180°) through the Kapton probe, in increments of 10°. Error bars represent one SD.

plane-parallel chamber such as the Roos chamber for QA dosimetry in external photon radiotherapy beams. The most significant variation recorded between the Roos chamber and the reference Geant4/CC13 data was a 4.35% over-response at a depth of 1 mm. Similarly, to the biased a-Si:H detectors on Kapton, its response downstream of $d_{max}$ is confined to a much closer agreement to the CC13, varying by no more than ± 0.8%. The PDD response of the Roos chamber and the a-Si:H detectors under bias are comparable for all depths investigated.

### 3.3.2 | Dose per pulse (DPP)

The DPP response, indicating dose-rate dependence of a-Si:H detectors, is presented in Figure 3. The DPP was obtained for the 5 μm thick detector with a 2 × 2 $mm^2$ sensitive area. Measurements were taken under a 3.5 V reverse bias before any significant delivered dose (i.e., no pre-irradiation). For a-Si:H detectors on glass substrates in MV fields, the authors have previously demonstrated that the DPP response in passive or photovoltaic mode (0 V) is poorer than under bias.[16] Hence, no unbiased results are presented in this study. Comparing the response of the a-Si:H detectors on glass from Large et al.[16] to the detectors on Kapton from this work, we see an extremely close agreement between the two data sets. This demonstrates that the transfer of the a-Si:H detector architectures to a flexible Kapton substrate has not affected the DPP response of the detector. As was observed in the authors' previous work,[16] both an applied voltage and a substantial pre-irradiation are required to remove the over-response observed at the lower DPP values. For a delivered DPP of 4.28 × $10^{-5}$ Gy/pulse, the a-Si:H detector on Kapton with 0 kGy pre-irradiation returns a response 51 % higher than under reference conditions (i.e., 2.78 × $10^{-4}$ Gy/pulse). On glass, the non-irradiated detector at 2 V produces a 38 % over-response at a DPP of 4.74 × $10^{-5}$ Gy/pulse. With a pre-irradiation of 10–20 kGy, the response of the a-Si:H detector on glass reduces to less than 1 % under-response at 4.74 × $10^{-5}$ Gy/pulse.

### 3.3.3 | Output factor

The OF results are given in Figure 9 for device aSiH-KAP5S for 0 and 2 V applied biases. The smallest pixel size was selected to minimize potential volume-averaging effects in small fields. Measurements at each field size are normalized to the response observed at 10 × 10 $cm^2$. The OF response of aSiH-KAP5S is benchmarked against the response of CC04 and CC13 ionization chambers used for QA at the SCCC. For all field sizes between 2 × 2 $cm^2$ and 20 × 20 $cm^2$, the a-Si:H detector, when operated at a 2 V reverse bias, produces an OF response that varies by less than 2 % from that of the CC04 and CC13 ICs, and by less than 1 % for measurements at 0 V. The most significant variations are observed at the smaller fields, with a 1.67 %

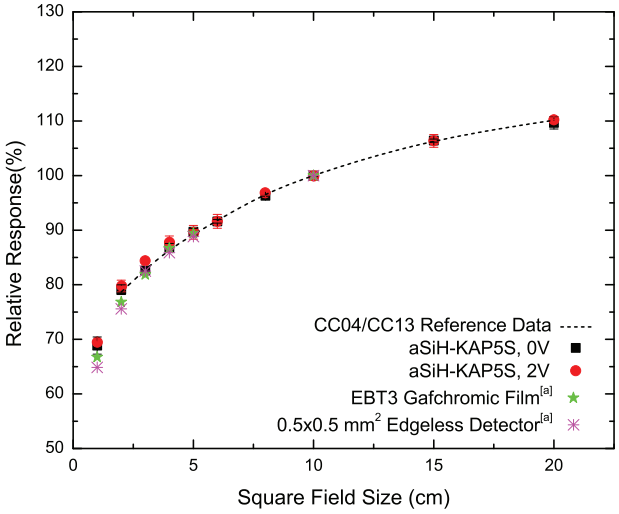


**FIGURE 9** Energy dependence of 5 μm a-Si:H single-pixel detectors. Responses are normalized to the response under 6 MV photons (1.2 MeV) from the LINAC. The ratio of mass absorption energy coefficient ($\mu_{en}/\rho$) for silicon over water (data from NIST[34]) is plotted for reference (solid line).

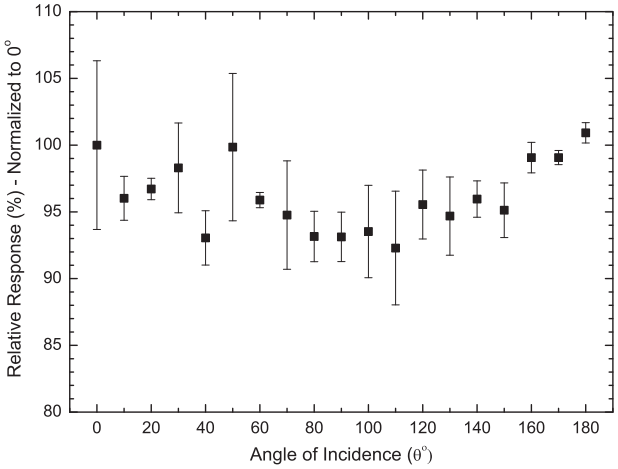


**FIGURE 10** Dependency of the device sensitivity on the applied bias. The results are given for 2.5 μm (red) and 5 μm (black) thick detector pixels with a 2 × 2 mm$^2$ sensitive area. The calculated fit equations from Equation (1) in Section 2.2.2 are displayed for each data series.

overresponse compared to the CC13 for a 3 × 3 cm$^2$ field and under 2 V bias. For 0 V bias, the most significant disagreement is a 0.55% overresponse against the CC13, which occurs for a 4 × 4 cm$^2$ field. Data taken from Petasecca et al. also presents the OF response EB3T Gafchromic film and an edgeless p-Si detector.[13] For fields between 2 × 2 cm$^2$ and 5 × 5 cm$^2$ the most significant deviation of the Gafchromic film and edgeless detector from the ICs is recorded as −1.85% and−3.11 %, respectively. Therefore, the a-Si:H results of Figure 9 are comparable in response to the reference CC04 and CC13 ICs and other dosimetry solutions.

### 3.3.4 | Angular dependence

The angular dependence of detector aSiH-KAP2S is displayed in Figure 10. The maximum angular dependence was observed at a 110° irradiation angle, which returned a response (7.71 ± 4.26)% lower than was recorded at 0° for radiation normally incident on the top surface of the detector. For irradiation incident on the backside of the detector (180° angle of incidence), the recorded response has minimal variation against the response at 0°, with a difference of only 0.92%. This demonstrates the transparency of the flexible Kapton substrate to MV x-rays, as no substantial attenuation of the signal has occurred. This feature is incredibly desirable for applications such as in vivo dosimetry where irradiations from the underside of the device may occur.

It should be noted that relatively large error bars, representing the standard deviation between repeated measurements, are present in this data. This is due to substantial variations observed over the repeated irradiations at each angle, facilitated by increased pressure on the device due to the detector phantom being slightly too small. Regardless, the angular dependence of these a-Si:H detectors on Kapton demonstrates an excellent response contained within ± 10%.

### 3.3.5 | Energy dependence

The energy dependence of 5 μm thick a-Si:H detectors was measured for low energy keV photons at the surface of a 10 cm thick water equivalent plastic and irradiated by a Gulmay kilovoltage x-ray machine. For comparison, the mass-energy absorption coefficient of silicon to water is extracted from the standard reference database of the National Institute of Standards and Technology (NIST).[34]

The energy dependence of the a-Si:H detectors shown in Figure 4 reproduce the general exponential trend for the energy dependence of crystalline silicon from NIST. We observe a lessened energy dependence for mean photon energies below 100 keV for all three measurement cases compared to the crystalline silicon reference data. For the lowest 49.97 keV mean photon energy (100 kVp), aSiH-KAP5S at 3.5 V bias records a 435% higher response than is recorded under reference dosimetry conditions and irradiated with 1.2 MeV mean energy photons. Between the biased and unbiased operation of aSiH-KAP5S, there is marginally lower energy dependence when operated passively, returning a 344% overresponse at 0 V compared to the 435% overresponse, as mentioned earlier. For the unbiased operation of aSiH-KAP5S and aSiH-KAP5L, the larger 5 × 5 mm$^2$ pixel size of aSiH-KAP5L results in the lowest responses recorded at each mean photon energy. Again,

for the case of 49.97 keV mean energy photons, the overresponse is now limited to 331%.

## 4 | DISCUSSION

The detectors displayed exceptional dose linearity, returning $R^2$ values ranging from 0.9997 to 1 across the various detector thicknesses and sizes. The dose calibration factors of the detectors vary from (0.580 ± 0.002) pC/cGy for the thinner and smaller detector (2.5 μm, 2 × 2 $mm^2$) to (19.36 ± 0.10) pC/cGy for the largest and thickest detector (i.e., aSiH-KAP5L—see Table 2). The sensitivities scale appropriately with sensitive areas but do not scale directly with active layer thicknesses. For detectors operated at 0 V with a 5 μm active layer, the sensitivity of the 5 × 5 $mm^2$ pixel (aSiH-KAP5L) exceeded that of the 2 × 2 $mm^2$ pixel (aSiH-KAP5S) by a factor of 6.58. This increase corresponds to the area factor of 6.25 between the two detector size variants. Conversely, the increase in sensitivity from 2.5 μm thick to 5 μm thick for 2 × 2 $mm^2$ sensors is represented by a factor of approximately 5. Sensitivities for the detector variations tested are provided in Table 2. As demonstrated in Figure 6, the detectors are never fully depleted from the pulsed x-rays of the LINAC. This suggests that the charges generated by the incident MV photons and participating in the current signal induced at the electrodes are dominated by the charge at the superficial layers underneath the contacts. A potential explanation of this result relates to DBs within the intrinsic a-Si:H layer and close to the contact regions of the devices becoming occupied, affecting recombination time. Recombination time on charged DBs is 10−100 lower than on neutral DBs present in the central part of the device. For devices that are not fully depleted, there is a larger relative volume in the thicker devices that possess neutral DBs. In addition to this effect, intrinsic regions close to the doped layers are expected to be more defective, as described through the defect pool model of a-Si:H.

For Figure 7's DPP results, an overresponse with decreasing DPP is recorded, reaching a factor of 300 % for a DPP of 2.53 × $10^{-5}$ Gy/Pulse. The authors' previous work on identical a-Si:H detectors on glass substrates illustrates that this dependence has been previously observed and further demonstrates that this is more exaggerated for unbiased detector operations.[16] Moreover, Large et al.[16] shows that this overresponse can be mitigated by applying bias combined with a pre-irradiation of 10−20 kGy. Softening of the incident x-ray beam produces an energy dependence of this material, resulting in an overresponse (Figure 4). This overresponse is largest for beams with lower mean photon energies, with the small pixel under bias returning an overresponse of 435% for 100 kVp photons (49.97 keV mean energy) compared to the response under the 6 MV (1.2 MeV mean photon energy) field. Operating the detector passively (0 V bias) reduces this factor to 344% at 100 kVp, and using the larger 5 × 5 $mm^2$ a-Si:H detector further reduces this to 331%. At these low energies where overresponse is observed, the photoelectric effect dominates. To this extent, the results of the a-Si:H detectors are compared to the mass-energy absorption coefficient ratio of crystalline silicon over water, taken from the NIST standard reference database.[34] Figure 4 demonstrates that the a-Si:H detectors still display an overresponse for lower average photon energies, which is similar in trend yet less pronounced than the NIST data for crystalline silicon. This suggests that the thin 5 μm intrinsic layer and the water equivalent packaging adopted have marginally improved the water-equivalence of the a-Si:H detectors in direct comparison to crystalline silicon detectors. The NIST data used for comparison relates to crystalline silicon irradiated with monochromatic x-ray sources, as no such data exists for a-Si:H under polychromatic x-ray beams. Consequently, the mass attenuation coefficient of a-Si:H and crystalline silicon under the polychromatic x-ray beams of the LINAC and kilovoltage machine may vary from the reference data used as a benchmark.

An excellent agreement in the PDD response of a-Si:H detectors is displayed in Figure 8, benchmarked against the reference measurements provided via Geant4 for the build-up region and by the PTW 30013 Farmer IC from $d_{max}$ out to a 250 mm depth. For the detectors operated under applied bias, the responses vary marginally, with percentage differences of no more than ± 3%. The applied bias acts to improve the signal-to-noise ratio of the a-Si:H detectors, allowing for a more accurate determination of the integral response (above the baseline) in environments where the response is extremely low, such as the build-up region of the PDD. The most considerable discrepancy in the PDD responses is observed for detector aSiH-KAP5S at 0 V, which returns a deviation from the Geant4 reference data of 5.67% at a 3 mm depth. This point could potentially be an outlier, as all other data points upstream of $d_{max}$ match the Geant4 simulation data to within ± 3%. For unbiased detectors downstream of $d_{max}$, a systematic under-response is observed. Sizeable percentage differences for both 2 × 2 $mm^2$ and 5 × 5 $mm^2$ are observed for depths of 100 mm and greater, ranging between −3.56% and −4.41%. This observation can be related to the energy dependence of the a-Si:H, as the x-ray spectrum hardens at increasing depths, resulting in a decrease in response, as observed in Figure 4. However, this decreased response with depth due to hardening of the incident x-ray spectrum is potentially mitigated by the dose rate dependence observed in Figure 3, as a lower instantaneous dose rate at increased depths results in an overresponse of the a-Si:H. Therefore, variations in the PDD response are

attributed to a combination of the detectors' dose rate and energy dependencies.

When assessing the use of this technology for in vivo dosimetry, an important consideration is to assess the possible enhancement to the skin dose which may arise when placing the detector in between the patient and the treatment beam. Based on the water-equivalence and thickness of the materials used in the detector's fabrication (Section 2.1), we can estimate the detectors water-equivalent thickness as approximately 200 μm. Based on the PDD profile of the build-up region from the Geant4 simulation study of Vicoroski et al.[26] (Figure 8b), adding an additional 200 μm of water-equivalent material on the patient would increase the skin dose by approximately 25%. Although this increase is non-negligible, it is comparable to other in vivo technologies such as TLDs and MOSFETs.[35]

The angular dependence of the a-Si:H detector technology is quantified in Figure 10 for incident angles of 0° up to 180°. The Kapton substrate on which the a-Si:H detectors are deposited is effectively transparent to x-rays.[36] This results in an observed maximum angular dependence at 110 degrees with respect to the beam of −7.71%. Moreover, in irradiation from the back of the detector (at an angle of 180°), the recorded response is effectively identical to the response at 0°, with a difference of only 0.92%. This minimal angular dependence is an attractive feature for in vivo dosimetry applications where irradiations can occur from many angles.

A LINAC OF was measured using the small pixel ($2 \times 2$ mm$^2$) a-Si:H detectors with 2.5 and 5 μm thicknesses. The results presented in Figure 9 normalize the response of each field size to the reference $10 \times 10$ cm$^2$ field. The a-Si:H results are compared directly against the OF obtained with the CC13 ionization chamber employed at SCCC for OF QA measurements. Further comparisons between alternate dosimeter technologies are also provided in Figure 9, with the OF response of EBT3 Gafchromic film and the "Edgeless" silicon detector technology extracted from Petasecca et al.[13] For the 5 μm results under 0 and 2 V applied bias, an extremely close match is observed with respect to the reference CC13 IC data. This response parallels the EBT3 film and the "edgeless" detectors (within experimental errors) for field sizes from $4 \times 4$ up to $20 \times 20$ cm$^2$. More importantly, the a-Si:H detectors provide an improved response closely matching the ionization chamber results (CC04) for small fields of $3 \times 3$ cm$^2$ and less. This significant result demonstrates the field size independence of the $2 \times 2$ mm$^2$ a-Si:H detectors for small field dosimetry applications.

Finally, the flexibility of the detector technology was demonstrated through the results in Figure 7. The general trend observed indicated that for conditions where the detector is subject to bending at radii of curvature smaller than 10 mm, the detector's response begins to degrade. For an 8 mm bending radius of curvature, the detector photosensitivity was reduced to $(-4.9 \pm 0.6)$% of the flat detector response. However, such extreme bending scenarios would never occur during in vivo dosimetry applications. These results also showcase that the flat response has a minimal variation (within ± 1%) after the Kapton tail is uncompressed and returned to a flat position. Therefore, as the variation in photosensitivity for a-Si:H detectors is less than ± 3% for bending radii of 10 mm and greater, these detectors can be expected to conform to various surfaces of a patient's body for in vivo dosimetry, allowing calibration in standard conditions, with minimal deviations in device response. It is difficult to isolate the mechanisms which may be causing degradation with increased bending. Degradations could arise from the a-Si:H detector itself and from lifting the carbon-based paint and epoxy contacts during bending. Future work will aim to investigate this further and will evaluate the detector flexibility under x-rays rather than visible light, as was conducted in this study.

## 5 | CONCLUSION

A series of fully flexible a-Si:H radiation detectors, realized through the deposition of a-Si:H n-i-p diodes deposited directly on a Kapton substrate, have been characterized to assess their feasibility as dosimeters in therapeutic x-ray fields and for in vivo dosimetry. The optimal detector design for dosimetry in MV fields was identified to possess a 5 μm thick active a-Si:H layer and a $2 \times 2$ mm$^2$ pixel area. The thicker 5 μm detectors proved advantageous for PDD measurements as they allow an improved signal-to-noise ratio as indicated by a lower percentage variation from the benchmark PDD curves. Furthermore, the 5 μm detectors demonstrated a minimal impact on the flexibility of the detectors, with the response returning to within 1% of its original response after bending. Concerning pixel area, the smaller $2 \times 2$ mm$^2$ architecture minimized volume averaging effects and provided better performance for OF than the larger $5 \times 5$ mm$^2$ pixels. Detectors with a $2 \times 2$ mm$^2$ pixel area and a 5 μm thickness provided the closest agreement to the expected PDD profiles at ± 2.95% when biased at 2 V. In summary, these detectors demonstrate dosimetric performances that parallel the currently employed detectors for QA and dosimetry for external beam radiotherapy, with comparisons provided directly against Gafchromic film, a Farmer Type IC, the CC13 IC, and the PFD 3G-pSi diode. Hence, the flexibility and dosimetric performance of the a-Si:H detectors in this work display exciting potential for applications as real-time dosimeters for QA and in vivo dosimetry for external beam radiotherapy. To fully assess the capabilities of these detectors for in vivo dosimetry, a more in-depth study is required to assess more complex components such as dose reconstruction under bolus or in cavities,

angular dependence of the detector for surface irradiations, field effect, and effects of electron contamination on the detector accuracy. Future studies will be dedicated to providing a complete characterization of these flexible a-Si:H detectors for in vivo dosimetry and skin dosimetry.

## ACKNOWLEDGMENTS

The authors thank the Shoalhaven Cancer Care Centre (SCCC) and Illawarra Cancer Care Centre (ICCC) staff for their valuable time and assistance with measurements. We also thank N. Vicoroski and their team for providing access to the Geant4 data used for our PDD measurement validations. This work was conducted as part of the INFN HASPIDE project. M. J. Large is supported by the Australian Government Research Training Program (AGRTP) scholarship and the Australian Institute of Nuclear Science (AINSE) Post-Graduate Research Award (PGRA). A. Bashiri is sponsored by Najran University, Saudi Arabia. The following funding sources and grants assisted in this work: Australian Government Research and Training Program (RTP) scholarship (M.J. Large and A. Bashiri). Australian Institute of Nuclear Science and Engineering (AINSE) Post Graduate Research Award (ALNSTU12583). Istituto Nazionale di Fisica Nucleare Scientific Committee (3D-SIAM and HASPIDE projects). Istituto Nazionale di Fisica Nucleare Committee for Technology Transfer (INTEF-3D-SiAm project). The Swiss National Science Foundation (grant number 200021_212208/1).

## CONFLICT OF INTEREST STATEMENT

The authors have no relevant conflicts of interest to disclose.

## REFERENCES

1. Miften M, Olch A, Mihailidis D, et al. Tolerance limits and methodologies for IMRT measurement-based verification QA: recommendations of AAPM task group no. 218. *Med Phys*. 2018;45(4):e53-e83. doi:10.1002/mp.12810
2. Prabhakar R. Real-time dosimetry in external beam radiation therapy. *World J Radiol*. 2013;5(10):352-355. doi:10.4329/wjr.v5.i10.352
3. Teunen D. The european directive on health protection of individuals against the dangers of ionising radiation in relation to medical exposures (97/43/euratom). *J Radiol Prot*. 1998;18(2):133-137. doi:10.1088/0952-4746/18/2/009
4. Knöös, T. Lessons Learnt from Past Incidents and Accidents in Radiation Oncology. *Clin. Oncol.* 2017;29(9):557-561. https://doi.org/10.1016/j.clon.2017.06.008
5. Santos T, Ventura T. A review on radiochromic film dosimetry for dose verification in high energy photon beams. *Radiat Phys Chem*. 2021;179:109217. doi:10.1016/j.radphyschem.2020.109217
6. Brace OJ, Fuduli I, Alnaghy S, et al. A large area pixelated silicon array detector for independent transit in vivo dosimetry. *Appl Sci*. 2022;12(2):537. doi:10.3390/app12020537
7. Olaciregui-Ruiz I, Beddar S, Greer P, et al. In vivo dosimetry in external beam photon radiotherapy: requirements and future directions for research, development, and clinical practice. *Phys Imaging Radiat Oncol*. 2020;15:108-116.doi:10.1016/j.phro.2020.08.003
8. Archer J, Li E, Petasecca M, et al. Synchrotron x-ray microbeam dosimetry with a 20 micrometre resolution scintillator fibre-optic dosimeter. *J Synchrotron Radiat*. 2018;25(3):826-832. doi:10.1107/s1600577518003016
9. Posar JA, Davis J, Large MJ, et al. Characterization of an organic semiconductor diode for dosimetry in radiotherapy. *Med Phys*. 2020;47(8):3658-3668. doi:10.1002/mp.14229
10. Large MJ, Posar JA, Mozer AJ, et al. Flexible polymer x-ray detectors with non-fullerene acceptors for enhanced stability: toward printable tissue equivalent devices for medical applications. *ACS Appl Mater Interfaces*. 2021;13(48):57703-57712. doi:10.1021/acsami.1c16914
11. Hachadorian RL, Bruza P, Jermyn M, et al. Imaging radiation dose in breast radiotherapy by x-ray CT calibration of Cherenkov light. *Nat Commun*. 2020;11:2298. doi:10.1038/s41467-020-16031-z
12. Zhu TC, Ong Y, Sun H, et al. Cherenkov imaging for Total Skin Electron Therapy—an evaluation of dose uniformity. In *Proceedings SPIE 11628, Mechanisms and Techniques in Photodynamic Therapy and Photobiomodulation*, 116280R. 2021. doi:10.1117/12.2583939
13. Petasecca M, Alhujaili S, Aldosari AH, et al. Angular independent silicon detector for dosimetry in external beam radiotherapy. *Med Phys*. 2015;42(8):4708-4718. doi:10.1118/1.4926778
14. Jeong S, Cheon W, Shin D, et al. Development of a dosimetry system for therapeutic x-rays using a flexible amorphous silicon thin-film solar cell with a scintillator screen. *Med Phys*. 2022;49(7):4768-4779. doi:10.1002/mp.15664
15. Street RA. *Hydrogenated Amorphous Silicon*. Cambridge University Press; 2005.
16. Large MJ, Bizzarri M, Calcagnile L, et al. Hydrogenated amorphous silicon high flux x-ray detectors for synchrotron microbeam radiation therapy. *Phys Med Biol*. 2023;68(13):135010. doi:10.1088/1361-6560/acdb43
17. Talamonti C, Large M, Pallotta S, et al. PD-0898 first dosimetric characterization of an a-Si:H dosimeter on flexible support. *Radiother Oncol*. 2023;182(1):S744-S745. doi:10.1016/s0167-8140(23)09023-0
18. Menichelli M, Bizzarri M, Boscardin M, et al. Testing of planar hydrogenated amorphous silicon sensors with charge selective contacts for the construction of 3D-detectors. *J Instrum*. 2022;17(03):C03033. doi:10.1088/1748-0221/17/03/c03033
19. Fuduli I, Porumb C, Espinoza AA, et al. A comparative analysis of multichannel data acquisition systems for quality assurance in external beam radiation therapy. *J Instrum*. 2014;9(06):T06003. doi:10.1088/1748-0221/9/06/t06003
20. Menichelli M, Bizzarri M, Boscardin M, et al. Fabrication of a hydrogenated amorphous silicon detector in 3-D geometry and preliminary test on planar prototypes. *Instruments*. 2021;5(4):32. doi:10.3390/instruments5040032
21. Li HU, Jackson TN. Flexibility testing strategies and apparatus for flexible electronics. *IEEE Trans Electron Devices*. 2016;63(5):1934-1939. doi:10.1109/ted.2016.2545706
22. Saleh R, Barth M, Eberhardt W, Zimmermann A. Bending setups for reliability investigation of flexible electronics. *micromachines*. 2021;12(1):78. doi:10.3390/mi12010078
23. Ernst D, Zerna T, Wolter KJ, Influences of organic materials on packaging technologies and their consideration for lifetime evaluation. In *Proceedings of the 2011 34th International Spring Seminar on Electronics Technology (ISSE)*. IEEE. 2011. 288-293. doi:10.1109/ISSE.2011.6053875
24. Happonen T, Häkkinen J, Fabritius T. Cyclic bending reliability of silk screen printed silver traces on plastic and paper substrates. *IEEE Trans Device Mater Reliab*. 2015;15(3):394-401. doi:10.1109/TDMR.2015.2457231

25. Schneider CA, Rasband WS, Eliceiri KW. NIH image to imagej: 25 years of image analysis. *Nat Methods*. 2012;9(7):671-675. doi:10.1038/nmeth.2089
26. Vicoroski N, Espinoza A, Duncan M, et al. Development of a silicon diode detector for skin dosimetry in radiotherapy. *Med Phys*. 2017;44(10):5402-5412. doi:10.1002/mp.12469
27. Oborn BM, Williams M, Bailey M, Carolan MG. IMRT treatment monitor unit verification using absolute calibrated BEAMnrc and Geant4 Monte Carlo simulations. *J Phys Conf Ser*. 2014;489:012020. doi:10.1088/1742-6596/489/1/012020
28. International Atomic Energy Agency (IAEA). *The use of plane-parallel ionization chambers in high-energy electron and photon beams: An International Code of Practice for Dosimetry*. Technical Report Series no. 381, 1997.
29. International Atomic Energy Agency (IAEA). Absorbed Dose Determination in External Beam Radiotherapy: An International Code of Practice for Dosimetry Based on Standards of Absorbed Dose to Water. Technical Report Series no. 398, IAEA, Vienna. 2000.
30. Wilkins D, Li XA, Cygler J, Gerig L. The effect of dose rate dependence of p-type silicon detectors on linac relative dosimetry. *Med Phys*. 1997;24(6):879-881. doi:10.1118/1.597985
31. Wong JH, Fuduli I, Carolan M, et al. Characterization of a novel two dimensional diode array the "Magic plate" as a radiation detector for radiation therapy treatment. *Med Phys*. 2012;39(5):2544-2558. doi:10.1118/1.3700234
32. Sauer OA, Wilbert J. Measurement of output factors for small photon beams. *Med Phys*. 2007;34(6 Part 1):1983-1988. doi:10.1118/1.2734383
33. Khan FM. *The Physics of Radiation Therapy*. 3rd ed. Lippincott Williams & Wilkins; 2003.
34. Hubbell JH, Seltzer SM, X-Ray Mass Attenuation Coefficients: NIST Standard Reference Database 126. National Institute of Standards and Technology, USA [Database]. 2004. doi:https://www.nist.gov/pml/x-ray-mass-attenuation-coefficients
35. Alnawaf H, Butson M, Yu PKN. Measurement and effects of MOSKIN detectors on skin dose during high energy radiotherapy treatment. *Australas Phys Eng Sci Med*. 2012;35:321-328. doi:10.1007/s13246-012-0153-1
36. Wu X, Shu C, He X, et al. Optically transparent and thermal-stable polyimide films derived from a semi-aliphatic diamine: synthesis and properties. *Macromol Chem Phys*. 2020;221(5):1900506. doi:10.1002/macp.201900506

## SUPPORTING INFORMATION

Additional supporting information can be found online in the Supporting Information section at the end of this article.

**How to cite this article:** Large MJ, Bashiri A, Dookie Y, et al. Characterization of a flexible a-Si:H detector for in vivo dosimetry in therapeutic x-ray beams. *Med Phys*. 2024;51:4489–4503. https://doi.org/10.1002/mp.17013